DERIVATION OF A WIND TUNNEL CONFIGURATION FOR A MID-RANGE AIRCRAFT WITH REAR-MOUNTED BLI ENGINES

M. Zeitler*, B. Britto*, P. Scholz*, R. Radespiel*, N. Iyer†, J. Friedrichs†, J. Schlittenhardt‡, J. Mangold‡, A. Strohmayer‡
* TU Braunschweig, Institute of Fluid Mechanics, Hermann-Blenk-Straße 37, 38108 Braunschweig, Germany
† TU Braunschweig, Institute of Jet Propulsion and Turbomachinery, Hermann-Blenk-Straße 37, 38108 Braunschweig, Germany
‡ University of Stuttgart, Institute of Aircraft Design, Pfaffenwaldring 31, 70569 Stuttgart, Germany

Abstract

Comprehensive evaluations of the Boundary Layer Ingestion technology require in-depth analysis of both, numerical flow simulations and meaningful experiments in wind tunnels. the latter are needed for validating various models employed in flow simulations. Therefore, wind tunnel experiments must be designed to represent the flow physics of the intended technology. This study focuses on the differences occurring in a wind tunnel compared to a full-scale configuration and how to derive a model that is representative of the design point. For this purpose, numerical simulations have been carried out for both conditions to be compared. While geometrical scaling has been employed, to scale the boundary conditions of the engine, two different approaches, Mach similarity and keeping the u-velocity ratio at freestream and fan face identical, have been investigated. The results show, that using a Mach similarity at the fan face to scale the boundary conditions generated larger shock strengths for the model configuration in conjugation with a lower inlet distortion coefficient compared to the full-scale case. The velocity scaling approach matched better in this regard, as well as when comparing the overall flow field near the fan. However, it sacrifices the need to keep the tip Mach number of the propulsive fan identical between the model and the full-scale configuration. Both model set-ups could not capture potential shock development at the start of the inlet ramp, making it important to carefully monitor inlet ramp flows when designing a suitable geometry, as this significantly impacts the fan distortion and local flow field.

Keywords

Boundary Layer Ingestion; Wind tunnel test

1. INTRODUCTION

A concept to further increase propulsive efficiency without necessarily changing the engine dimensions is the boundary layer ingesting (BLI) engine. The fundamentals of this concept in the field of aviation have been known for several decades, dating back at least to Smith [1]. Taking inspiration from the naval sector, the underlying idea is to intake the slow moving air of the boundary layer into the engines and re-energizing it. This effectivley reduces the wake losses as the dissipative losses of airframe wake and propulsive jet surpass the combined loss of the BLI configuration, ultimately reducing the required mechanical flow power. This allows for a decrease in engine mass flow and/or jet velocity [2]. The first choice would enable a smaller engine and, therefore, a reduction in weight. The latter leads to a decrease in jet dissipation [2]. In response to the above stated emission goals as well as the cost reduction that follows a decrease in fuel consumption, BLI has gained in attention over the last few years, resulting in different concepts to integrate engines into e.g. the fuselage. According to the propulsor integration strategy, these concepts can be distinguished:

- BLI engines with a full 360° ingestion, as shown in the upper part of figure 1
  These concepts place an engine aft of the tail of a fuselage-wing configuration. The engine takes in boundary layer around its full circumference. This reduces the non-uniformity at the fan-plane compared to other BLI-configurations, therefore offering better fan performance. On the downside, due to safety and power requirements, the single BLI propulsor is only an addition to under-wing engines, and hence, leads to an increase of propulsion complexity and weight of the propulsion system. These concepts are referred to as BLI360.
- BLI engines with only a part of the inlet ingesting boundary layer, examples depicted in the bottom two image parts of figure 1
  While the distortion is higher in these configurations, the integrated engines fully replace any under-wing propulsor. Concepts using this approach are often referred to as BLI180 (although the engine section intaking boundary layer doesn't have to be 180°). Only partially integrated engine strategies are often combined with new and innovative airframe designs, such as the D8 from MIT [3] shown in figure 2a or the conceptional design of Airbus's blended wing body with distributed propulsors [4] seen in figure 2b

While there exist a vast variety of studies including BLI, there are still many aspects unknown. As pointed out by Moirou et al. [5] in 2023, especially the BLI180 configurations still lack thorough optimization studies. Another mostly blank area are the occurring flow phenomena and the impact on the flow field by embedding the engine into the fuselage, as well as how different geometrical aspects of the integration have an influence on the resulting propulsive efficiency.

The DFG-funded research programme SynTrac investigates different synergies in highly integrated aircraft configurations. Parts of that programme focus on a conventional tube-wing approach but with integrated engines at the rear of the fuselage to study BLI behavior, not only using numerical methods, but wind tunnel experiments as well. As experiments mostly can't be performed at full-scale, especially when applying not

doi: 10.25967/630305

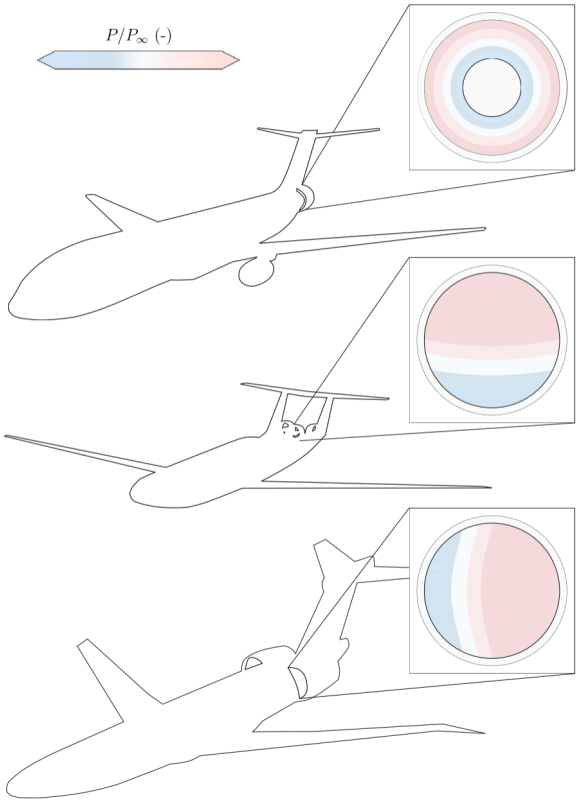

FIG 1. Schematic of governing distortion types (normalized total pressure) for various embedded propulsion systems [5]

(a) MIT's D8 [3]

(b) Airbus's ZEROe BWB concept [4]

FIG 2. Innovative airframe concepts including integrated engines

yet adapted concepts, down-scaling of promising geometries to allow for model/wind tunnel testing is necessary.
As kinematic similarity can't be achieved in all aspects, this study investigates the differing flow fields at the fan inlet of a wind tunnel and full-scale BLI-configuration, using numerical methods. The aircraft used is based on a mid-range civil transport aircraft with a mid-cruise speed of $Ma = 0.78$. The propulsors are embedded in the rear of the fuselage. Different parameter variations of the engine integration aspects are simulated at both model and full-scale conditions. This allows to highlight the challenges to overcome when creating a BLI180 configuration at wind tunnel and full-scale conditions and provides insights into how to derive a suitable model in the future.

NOMENCLATURE

Symbols

A	fan intake area	m^2
α	angle of attack	deg
C_p	pressure coefficient	-
D	fan tip diameter	m^2
N	fan speed	rpm
ν	hub to tip ratio	-
p	pressure	Pa
q	dynamic pressure	Pa
r	radius	m
Re	Reynolds number	-
T_t	total Temperature	K
$\dot{V}$	volumetric flow rate	m^3/s
x	x-coordinate	m

Indices

60	60 °section
design	full scale configuration
model	model configuration
e	engine
f	fuselage
tip	fan tip
tot	total

Abbreviations

AoA	Angle Of Attack	°
BLI	Boundary Layer Ingestion	
BPR	Bypass Ratio	
CD	Discharge Coefficient	
CFG	Specific Thrust Coefficient	

DC60	Inlet Distortion Coefficient	
DOE	Degree Of Embedding	
FPR	Outer Fan Pressure Ratio	
Ma	Mach number	
OPR	Overall Pressure Ratio Ratio	
PAX	Passengers	
RANS	Reynolds Averaged Navier Stokes	
SFC	Specific Fuel Consumption	
T4	Burner exit temperature	K
TLARs	Top Level Aircraft Requirements	
UHBR	Ultra high bypass ratio	
V1	Inlet Spline Variation 1, standard CATIA spline	
V2	Inlet Spline Variation 2, iCST approach	

2. METHODS

2.1. Geometrical Models

2.1.1. Aircraft Configuration

The configuration used in this study, shown in a simplified version and without any engines in figure 3, is based on the top-level aircraft requirements (TLARs) of an A320neo. For

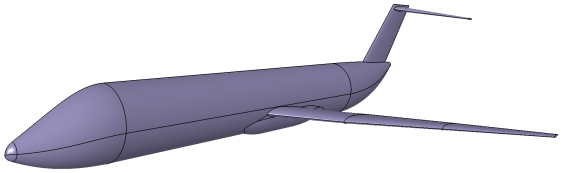

FIG 3. Simplified SynTrac 1a configuration without engines

the preliminary aircraft design, a modified in-house (IFB, University of Stuttgart) version of SUAVE is used. Listed in table 1, are the main geometrical parameters, as well as the TLARs of the aircraft. In contrast to an actual A320neo, the engines are embedded at the rear of the fuselage, requiring the adaptation of a T-tail. The concept allows for varying integration details of BLI-180 engines. To ensure safety in case of a rotor burst, an 80 cm thick area in the center of the fuselage limits the maximum integration depth at any position.

2.1.2. Parameterized Integration

The embedding of the reference engine into the fuselage is fully parameterized, including

- the nacelle
- the horizontal and vertical engine position
- the inlet length and width
- integration depth
- the engine highlight radius at the fuselage connection
- the length of the nacelle-fuselage connection
- the spline defining the center s-curve of the inlet surface

SynTrac BLI Configuration	
Fuselage length	37.5 m
Wing span	34.83 m
Mean aerodynamic chord	3.99 m
Wing area	115.83 m^2
Cruise speed	0.78 Ma
Cruise altitude	10668 m
PAX	180

TAB 1. Top Level Aircraft Requirements and geometrical data of the SynTrac BLI Configuration

- the pitch and yaw angle of the engine
- multiple additional aspects related to connecting the nacelle to the fuselage

This extensive parametrization allows for a vast variety of geometries to be created. For this paper, only the inlet length, the center spline, the inlet width as well as the nacelle shape itself were varied, as shown in figure 4. Upstream of the inlet, the fuselage of the aircraft configuration has not been altered.

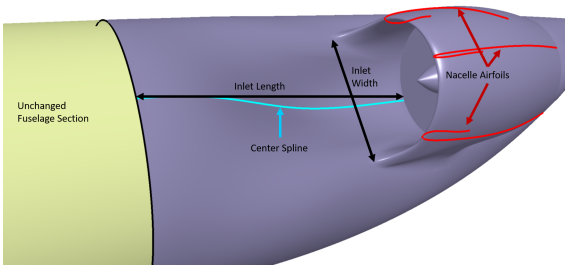

FIG 4. Selection of inlet parameters

Important fixed parameters are listed in table 2. Both the horizontal and vertical engine positions are measured from the nose of the fuselage and are based on the preliminary aircraft design.

Horizontal engine position	31 m
Vertical engine position	1.2 m
Degree of embedding	0.722

TAB 2. Important fixed parameter values

The degree of embedding (DOE), as described by Vinz and Raichle [6], being the ratio of masked diameter to total diameter as visualized in figure 5, was chosen to be the maximal possible value at the given position with respect to geometrical constraints. Specifically, the safety zone in case of a rotor burst of 80 cm width in the center of the fuselage was the limiting factor.

$$DOE = \frac{r_e + r_f - l_e}{2 \cdot r_e} \tag{1}$$

The chosen degree of embedding was based on the findings of Vinz and Raichle [6] as well as the theoretical approach by Hall et al. [2], stating, that a higher degree of embedding potentially yields a larger benefit of BLI. While this doesn't take the fan distortion and its negative effects into account, it was used as the baseline of this study.

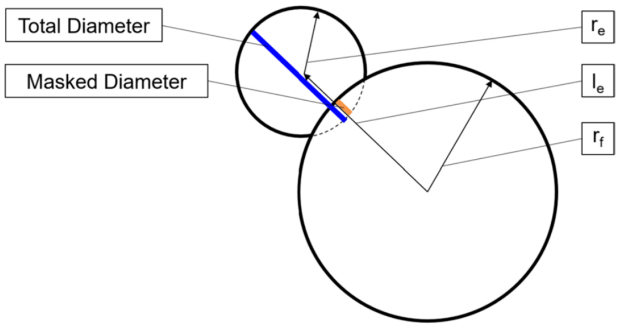

FIG 5. Definition of degree of embedding (DOE) [6]

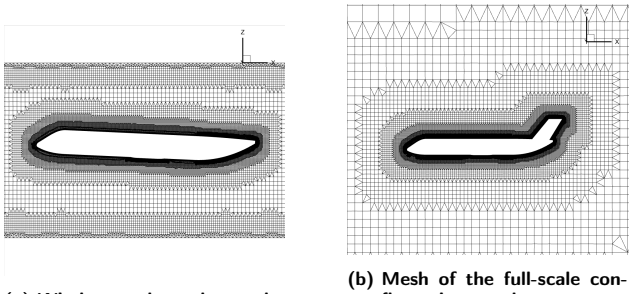

(a) Wind tunnel mesh at the symmetry plane

(b) Mesh of the full-scale configuration at the symmetry plane

FIG 6. Comparison of the volume meshes at the symmetry plane

2.2. Numerical set-up

2.2.1. Mesh

The meshes for the simulations were created using Pointwise, being a hybrid of structured and unstructured domains. A y+ value of <1 was achieved for the vast majority of surface cells in both the full-scale and model case. The total number of surface cells on the aircraft was kept as similar as possible between the two set-ups, displayed in figure 6. The full-scale configuration was meshed in some areas slightly finer to compensate for the larger difference in surface cell scales to the first cell layer height to achieve y+<1. The volume meshes of the two set-ups differ due to the farfield or wind tunnel walls respectively, as can be seen in figure 6a for the model and in figure 6b for the full-scale configuration. Depicted in both cases are the meshes on the symmetry plane.

2.2.2. Boundary Conditions

For the aircraft surfaces, a viscous wall boundary was set. The flow state of the engine inlet at the fan plane is defined by specifying a fixed mass flow. The bypass and core exit are defined by temperature and pressure ratios. The latter are adjusted within the simulation to adapt to a specified mass flow. In case of the wind tunnel model, the wind tunnel walls are specified as Euler walls, while the flow around the full-scale configuration is defined by specifying suitable farfield conditions. For the tunnel in- and outlet, the pressure at outflow and suitable flow conditions at the inflow boundaries are prescribed. An angle of attack of 2.6° was set for the full-scale configuration, while the aircraft itself was rotated by the same amount in the wind tunnel to achieve an identical angle of attack. The reference values for each set-up are listed in table 3:
The boundary conditions for the engine specifically are listed in section 3, covering the propulsor design itself.

	full-scale Configuration	Wind tunnel Configuration
Reference Ma	0.78	0.14 (50 m/s)
Temperature [K]	228.8	298
Density [kg/m^3]	0.363	1.184
Pressure [bar]	0.24	1.01

TAB 3. Set-up reference values

2.2.3. Numerical solver

The DLR-TAU code was used for the simulations, which allows solving the RANS equations on unstructured meshes [7]. Settings were based on the study of Vinz and Raichle [6] with the spatial discretization of the convective fluxes being chosen to be a central differences scheme with matrix dissipation. Central difference discretization for the viscous fluxes and an implicit Euler method to solve the steady-state equations were employed. For solving the linear system, a LUSGS method was used. Differing from the mentioned study, the SST-kω model was chosen to model the turbulence instead of Spalart-Allmaras, as it is a more physics based model, and a small convergence study did not show any significant computation time difference between the two.

3. BASELINE ENGINE DESIGN

The first step in understanding the synergies arising from such a high level of airframe-propulsor integration is the design and sizing of a baseline engine and its corresponding aerothermodynamic cycle. To align with the trend of increasing bypass ratios (BPR) that drives reduction in specific fuel consumption (SFC), a UHBR engine with a BPR of 18 was chosen. A higher BPR was not considered, as SFC improvements plateaued beyond a BPR of 19, offset by the increased takeoff weight, particularly due to the larger fan module. The engine design was done using Gasturb® in accordance with the top level aircraft requirements (TLARs) as shown in table 4. With the aim of minimizing engine sizing and ability to accommodate off-design operation, mid-cruise was selected as the design cycle point. Parametric studies were further implemented to determine the most feasible engine design parameters.

Operating Point	Altitude	Mach Number	Thrust Setting
	m	-	kN
Takeoff	0	0	120
2nd Segment OEI	0	0.24	80
Climb 4000ft/min	457	0.4	80
Initial Cruise Altitude	10058	0.76	24
Mid-Cruise	10668	0.78	21
Service Ceiling	11887	0.78	24
Ceiling OEI	7620	0.557	49

TAB 4. TLARs used for Engine Design

A two-spool geared unmixed-flow turbofan engine was selected over a direct-drive turbofan because incorporating a gear system between the low-pressure turbine and the fan

allows for lower fan pressure ratios. A gear ratio of 3.144 was chosen, following the engine design study by Giesecke et al. [8], which involved the over-wing integration of a UHBR engine. The burner exit temperature (T4) was set at 1700K. It was observed that the temperature T4 at which minimum SFC was achieved, increased with the overall pressure ratio (OPR). Increasing OPR contributes positively to the engine core's thermodynamic efficiency at the cost of very low blade heights in the last stages of the high pressure compressor. In order to achieve a 5% improvement in SFC while maintaining manageable blade heights, the temperature T4 was reduced from 1800K to 1700K, with a core efficiency of 59%. Based on a sensitivity study examining the relationship between outer fan pressure ratio (FPR) and BPR, along with trends presented by Giesecke et al. [8] and Bijewitz et al. [9] OPR at 75 and FPR at 1.374 was chosen. The specific thrust coefficients (CFG) and discharge coefficients (CD) used to define the bypass and core nozzles were implemented based on the studies carried out by Benjamin et al. [10], with the objective of improving nozzle efficiency. The component efficiencies used to define the various propulsor submodules were obtained by extrapolating technological trends presented by Giesecke et al. [8] and Daggett et al. [11].

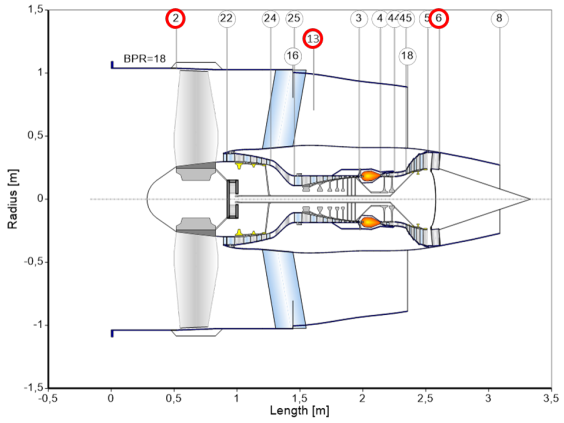

FIG 7. Geometry of UHBR18 engine with station numbering

The engine intake mass flow was modeled as an iterative parameter to meet the thrust requirements outlined in table 4. Using the aforementioned chosen engine parameters, Gasturb® generated a preliminary baseline geometry. This geometry was then further adapted to create a three-dimensional nacelle geometry, incorporating the axial positions of the different stations, as well as the area dimensions, as shown in figure 7. The final design used in this paper was determined by conducting a small design study, in which mainly the nacelle was varied. The study was focused on minimizing shock occurrence and preventing any significant separation areas. For these simulations, the engine was centered in a farfield domain, without any additional attachments. Figure 8 depicts the results of the isolated engine case with an angle of attack of 0° and 2.6° respectively. For shock indication, the mach number with ISO-surfaces of $Ma = 1$ are plotted. The contour plots in figure 8c and 8d show the x-velocity at the different AoA. The minimum values being 7 m/s and 2.5 m/s for $\alpha = 0$ °and 2.6 °respectively, indicating no occurring flow separation within the nacelle.
In addition to geometric data, the calculated thermodynamic cycle data for the design point were used to prescribe boundary conditions for the CFD setups of both the isolated engine case and the heavily buried propulsor-airframe configuration.

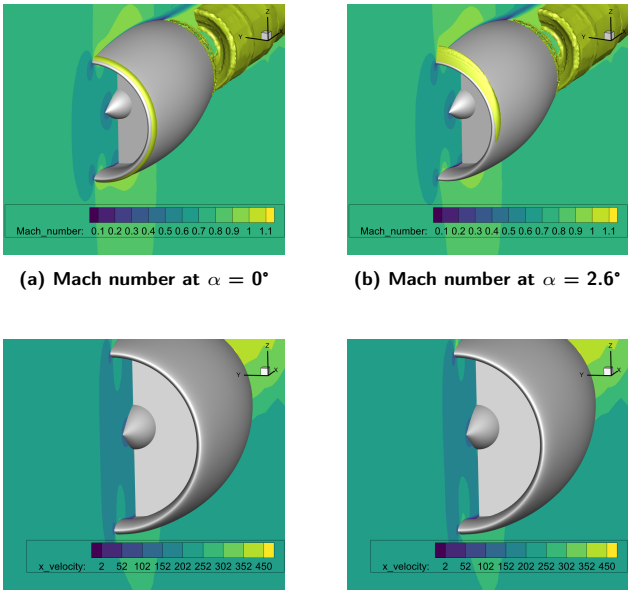

(a) Mach number at $\alpha = 0°$

(b) Mach number at $\alpha = 2.6°$

(c) Areas of negative x-velocity at $\alpha = 0°$

(d) Areas of negative x-velocity at $\alpha = 2.6°$

FIG 8. Preliminary nacelle and engine design

Fan Inlet	
Mass Flow Rate (kg/s)	251.89
Bypass Duct Inlet	
Mass Flow Rate (kg/s)	238.63
Total Pressure (Pa)	48908.6
Total Temperature (K)	271.19
Core Nozzle Inlet	
Mass Flow Rate (kg/s)	13.09
Total Pressure (Pa)	35984.3
Total Temperature (K)	625.42

TAB 5. Design point (Mid-Cruise) Boundary Conditions

The engine inlet (station 2) was prescribed by a fixed mass flow intake, while the outlets had a targeted mass flow rate that was achieved by iterating the pressure ratio. Station 13 is the outlet of the fan stage, which marks the start of the bypass duct and station 6, located after the exit guide vane, is the core nozzle exit. The total pressure and temperature boundaries from Gasturb as shown in table 5, were not directly translated into the CFD setup; rather, they were normalized by static pressure at the reference state and total temperature at the reference state, respectively.
As pointed out by Hall et al. [2], the exact boundary conditions for an embedded configuration differ from the isolated case. Especially the mass flow can be decreased, if the main geometrical engine parameters and flight conditions are kept constant, due to a decrease in losses. As the current study is at its very beginning, detailed information and required data for higher fidelity engine modeling within the CFD calculations was not possible. Additionally, this paper does not focus on the potential benefits BLI provides over conventional configurations, but instead aims at the derivation of a suitable wind tunnel configuration, based on comparison with a full-scale version. As the conditions were scaled between these two configurations and not compared to a conventional aircraft, the inaccuracy in setting up the boundary conditions was deemed negligible.

4. WIND TUNNEL MODEL

To study the effects of integrated engines, numerical simulations in combination with wind tunnel experiments are required, especially to validate simulation data. Due to the differing conditions of the full-scale aircraft flying at Mach 0.78, at an altitude of almost 11000 m and the wind tunnel, this paper focuses on how to derive a model configuration. The tunnel planned to be used (PTF-tunnel of the IFAS, TU Braunschweig) has a test section of 2.4 m x 2.4 m. Due to limitations in the engine scaling as well as to increase the Reynolds number of the model set-up, a clipped wing configuration with a scaling factor of 1:12.5 was chosen. Effects of clipping the model's wings will be discussed in section 4.2 The wind tunnel specifications are as stated below:

Flow velocity	50 m/s
Temperature	298 K
Density	1.184 kg/m^3
Wind tunnel cross-section	2.4 m x 2.4 m

TAB 6. Wind tunnel specifications

4.1. Engine scaling

The design in section 3 represents a full-scale aircraft engine operating at cruise. When scaling down the model, geometric scaling was maintained. Since the Reynolds number could not be preserved due to differences in operating Mach number and ambient conditions, two different scaling options for the engine conditions were chosen:
- Mach similarity as defined in equation 2
- Velocity ratio as defined in equation 4

The Mach similarity scaling keeps the fan tip Mach number identical for the full-scale and model configuration. This scaling can be labeled as an engine scaling, as it is important for fan behavior in isolated engine cases, as shown by Eggers [12].

The scaling by velocity ratio was chosen to keep the flow fields at the fan inlet identical between the full-scale and model cases. While this scaling does not account for the difference in Reynolds number, it preserves the velocity ratios of the x-velocity component between the freestream and the fan face.

$$\frac{N\sqrt{A}}{\sqrt{T_t}} = const. \qquad \frac{\dot{V}}{ND^3} = const. \tag{2}$$

with the fan area being

$$A = \pi r_{tip}^2 (1-\nu)^2, \tag{3}$$

$$\frac{u_{Fan,Full-Scale}}{u_{\infty,Full-Scale}} = \frac{u_{Fan,Model}}{u_{\infty,Model}} \tag{4}$$

Using the different scaling factors, the mass flow rate accounts for the following:

	Mach similarity	**Velocity ratio**
Mass flow rate [kg/s]	4.98	0.986

TAB 7. Different mass flow rates based on chosen scaling factors

4.2. Effects of clipping the wings

A preliminary study on the LEISA aircraft [13], a slightly different configuration than the one used for the main study of this paper, was conducted for a full-scale model in free stream flow with wind tunnel conditions and compared to simulation results of the wind tunnel set-up. The study was conducted at two different angles of attack, 0° and 5° for four different configurations, namely the configuration at free flight conditions and 3 configurations inside the wind tunnel set-up:
- Wing-Body Freestream
  full-scale configuration in free stream flow with wind tunnel conditions
- Wing-Body 100%
  A scaled down version by the factor of 22.22 with no changes to the wings. The model spans 3/4 of the wind tunnel width.
- Wing-Body 75%
  A scaled down version by the factor of 12.5 with clipped wings at 75% span length.
- Wing-Body 50%
  A scaled down version by the factor of 8.33 with clipped wings at 50% span length.

The clipped wing variations connect directly to the tunnel walls, as is planned for the intended wind tunnel experiments. The wind tunnel walls are considered to be Euler walls. To showcase the effects of scaling and clipping the wings, different parameter values are plotted against the angle of attack. Figure 9 shows that the lift coefficient is almost unaffected by scaling the aircraft, without clipping the wings. The small deviation is obviously caused by the classical interference effects of the closed-wall test section: Solid blockage and streamline curvature. For the clipped wings, the lift coefficient increases when the cutting plane shifts towards the wing root. Additionally to the above effects, since the wind tunnel walls themselves are considered to be Euler walls, according to potential flow theory, this effectively makes the airline model mirrored infinitely, leading to reduced induced downwash at the wing position and hence, the increase in lift coefficient.

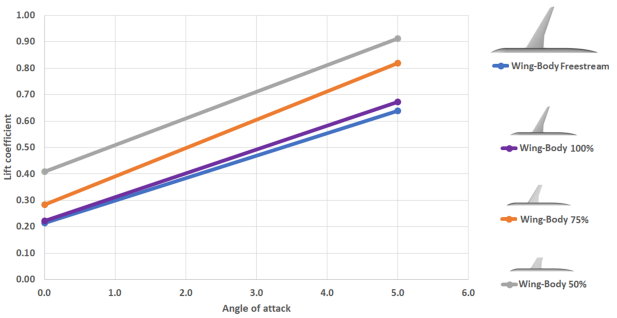

FIG 9. Effect of clipped wings on lift coefficient

Main focus of this study is to understand the flow near the engine inlet for which a suitable position has to be chosen as the LEISA wing-body configuration does not have a BLI inlet. From the baseline design shown in fig 3, the engine inlet plane was located approximately at 27% of the fuselage rear cone length. Therefore, a similar plane was chosen for the LEISA wing-body, and analysis of the local flow downwash has been performed at the center of the engine inlet.

With this set-up, the incidence angle at the fictional fan plane is plotted against the angle of attack in figure 10. A similar behavior as with the lift coefficient can be seen. Only a minor change is seen between the full-scale and the model version without clipped wings. As the cut-off section of the wing moves towards the wing root, the local incidence angle increases. This can be contributed to the lining effect of the wind tunnel walls due to which the flow below the airline model adjusts itself along the flow near the wind tunnel walls. As the angle of attack is increased, the trend continues but at a higher rate, indicated by steeper slopes. This is also supported by figure 11 plotting the downwash angle against the AoA. It is shown that, as the clipping of the wing moves towards the root, the effect of the AoA on the downwash angle slowly reduces. Therefore, though we increase the AoA, the downwash angle remains nearly constant for the Wing-Body 50% configuration. From the above comments, it is visible

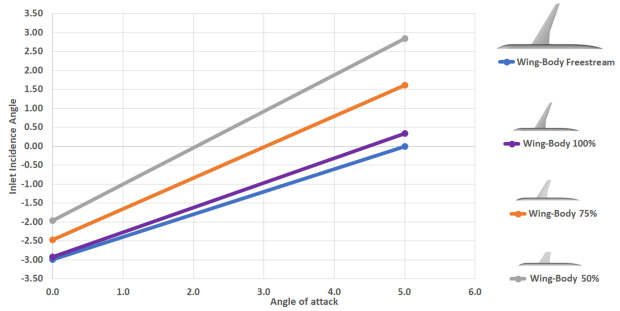

FIG 10. Effect of clipped wings on engine inlet incidence angle at a fictional fan plane

that the Wing-Body 75% configuration has similar effects as the full-scale model and Wing-Body 100% configuration on the engine inlet and downwash angle than that of the Wing-Body 50% configuration. Therefore, it is concluded that the 75% configuration is more suitable than the 50% one, as the former doesn't impact the flow behavior near the engine inlet region as much as the latter.

Applying a scaling factor of 12.5 to the SynTrac configuration leads to clipped wings of nearly 85% their span-wise extension, and therefore having only a minor change in the flow-field when compared to a model with complete wings.

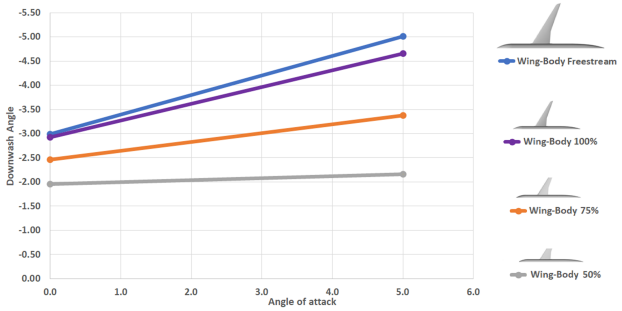

FIG 11. Effect of clipped wings on downwash angle at a fictional fan plane

5. RESULTS

5.1. Geometrical Variations

Specifically interested in the inlet area of the integrated engine, this study focuses on the rear part of the fuselage, where the engine is located, as shown in figure 12. Ingesting bound-

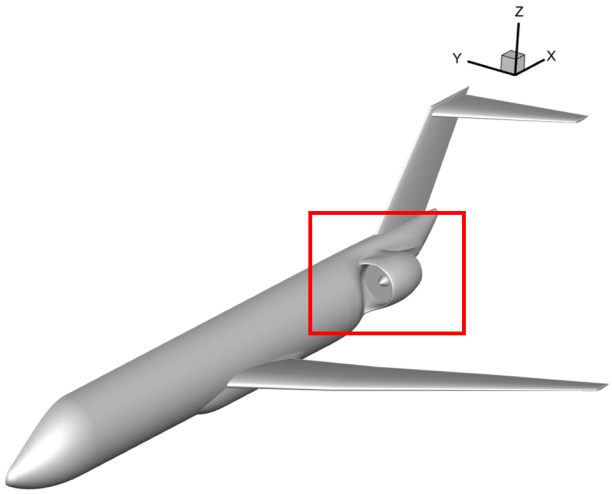

FIG 12. Area of Investigation

ary layer creates a blockage effect, effectively reducing the inlet area of the nacelle. In response, the mean velocity of the unaffected area has to increase in order to meet a certain mass flow. Shown in figure 13 are areas near the inlet reaching Ma = 1. While the jet velocity out of the engine as well as parts of the wing (blue area in the front part of the figure) reach the speed of sound, it can also be seen, that additional shocks form at the start of the inlet ramp, as well as a shock formation near the nacelle leading edge, directed inwards into the intake. While the first one is the result of a strong convex curvature of the chosen design, the latter is caused by the mentioned blockage effect of the boundary layer. The occurrence of the inlet shock was previously mentioned in literature, for example by Vinz and Raichle [6]. As this is a undesired flow phenomenon for turbofan engines, design efforts are needed for mitigation. To compensate for the blockage, the intake design is adjusted with a significant increase in its inlet area by almost 18% compared to the isolated engine case. Shown in figure 14 are the areas of Ma = 1 for two adapted geometries. The design shown in figure 14b employs a larger inlet length compared to 14a to mitigate the shock at the start of the intake ramp. This is due to the curvature being „stretched

out“. An increase in the inlet area significantly reduces the shock occurrence within the inlet, being fully eliminated for the design with a longer ramp. Additionally, this points out, that reaching Ma = 1 close to the nacelle leading edge of the inlet, augments the occurrence of the shock formation at the inner lip.

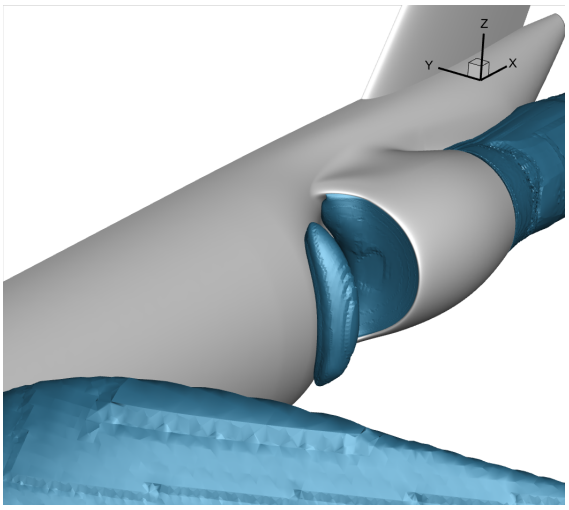

FIG 13. Areas reaching Ma = 1 in a full-scale configuration

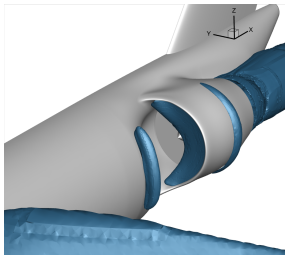

(a) Adapted full-scale configuration with a short inlet length of $L_{Inlet}/D_{Fan} = 1.89$

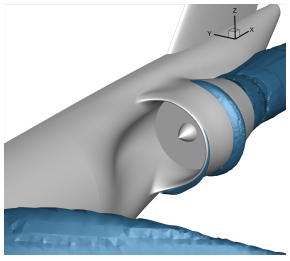

(b) Adapted full-scale configuration with a longer inlet length of $L_{Inlet}/D_{Fan} = 2.47$

FIG 14. Areas of Ma = 1 for different full-scale configurations

5.2. Comparison of full-scale and wind tunnel configurations

To derive a suitable wind tunnel model, comparison between the full-scale configuration and the model cases are being looked into. Shown in figure 15 are the areas of Ma = 1 for the full-scale configuration (figure 15a) with the longer inlet, as well as for its model cases with Mach similarity (figure 15b) and the velocity ratio (figure 15c) scaling applied. The model cases do not show any shock formation on the outer part of the nacelle, due to the much lower wind tunnel flow speeds. For the model with applied Mach similarity, areas reaching the speed of sound can be seen within the inlet. This is a clear distinction between the two scaling approaches, as for the velocity ratio scaling, no shock formations can be observed.

The x-velocity component normalized by $\overline{u}$ at the fan face is shown in figure 16 for the mentioned configurations. The overall flow field compared to the full-scale case shown in figure 16a matches best for the velocity ratio scaling depicted in figure 16c. This is to be expected, as this scaling is meant to preserve the u velocity ratios. However, it doesn't account for the difference in Reynolds number. For both the full-scale

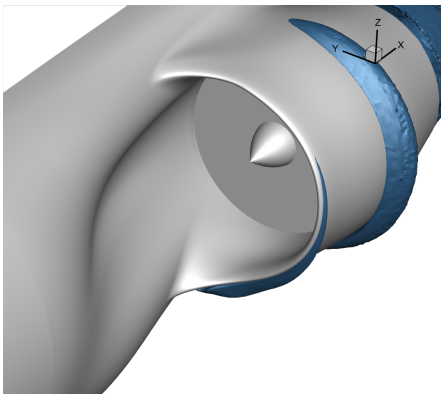

(a) Full-scale configuration with longer inlet

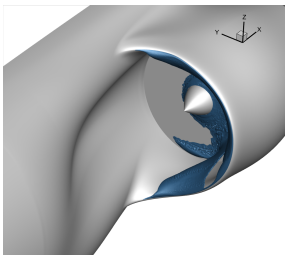

(b) Model configuration with Mach similarity scaling

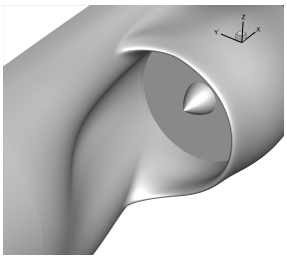

(c) Model configuration with velocity ratio scaling

FIG 15. Areas of Ma= 1 for full-scale and model configurations with longer inlets

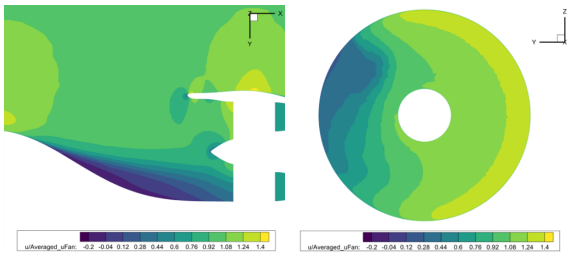

(a) Full-scale

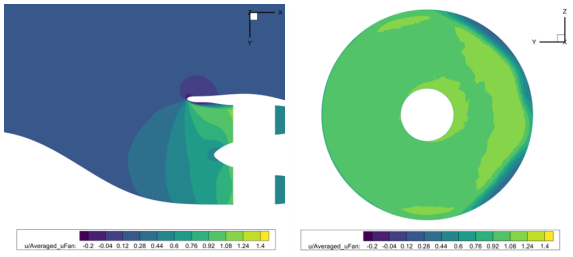

(b) Mach similarity model case

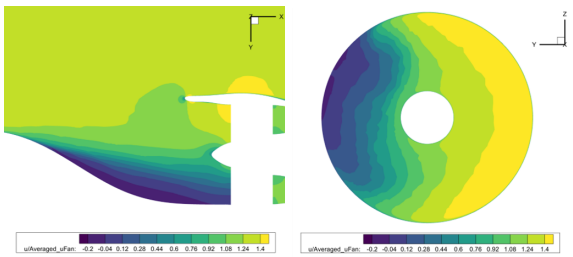

(c) Velocity ratio model case

FIG 16. $u/\overline{u}_{Fan}$ at horizontal plane through the engine center and for the fan plane

and the model with velocity ratio scaling, a separation area can be seen forming shortly after the steepest slope of the inlet ramp. For the case with Mach similarity shown in figure 16b, this is not the case. Instead, a strong acceleration towards the fan, due to the high specified mass flow rate, is visible.
For the design with a smaller inlet length, figure 17 shows the areas of Ma = 1. The shock at the start of the inlet ramp exists only in the full-scale configuration, accounted to the higher freestream velocity. The main aspect to be seen is, that the velocity ratio model case doesn't show any shock formation, despite their occurrence in both other configurations.

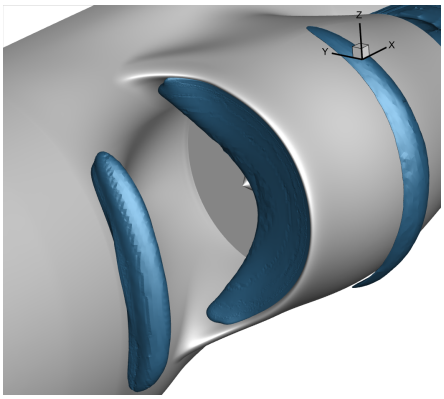

(a) Full-scale configuration

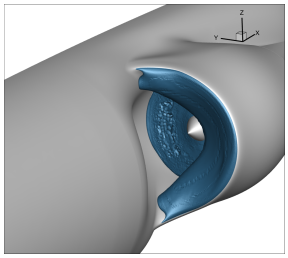

(b) Model configuration with Mach similarity scaling

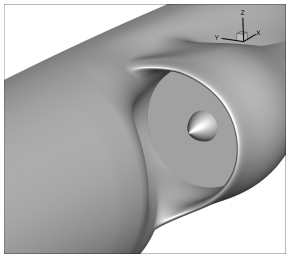

(c) Model configuration with velocity ratio scaling

FIG 17. Areas of Ma= 1 for full-scale and model configurations with shorter inlets

5.3. Inlet Distortion

The inlet distortion coefficient DC60 (see eq. 5) is an often used parameter (e.g. by Rodriguez [14] or Pecinka et al. [15]) to characterize distortion at the fan face.

$$DC60 = max\left(\frac{\overline{p}_{tot,Fan} - \overline{p}_{tot,60°,min}}{\overline{q}}\right) \tag{5}$$

It describes the deviation of the mean total pressure at the fan face $\overline{p}_{tot,Fan}$ to the minimum mean total pressure within a 60°section $\overline{p}_{tot,60°}$ and is being normalized by the mean dynamic pressure $\overline{q}$. Shown in figure 18 are the DC60 values for geometries with different inlet lengths in full-scale, as well as for the different model cases. The first thing to point out is the lower DC60 value at shorter inlet lengths for the full scale configuration. In these cases, shocks and potentially fully supersonic flow can be observed in the inlet. As there is no physical explanation as to why such a flow phenomena should reduce the distortion, it is reasonable to assume that this occurs due to the numerical set-up and the used boundary conditions. However, further detailed analysis will be needed to understand this phenomena. Additionally it has to be pointed out, that shock development or supersonic inflow in general is to be avoided, as it generates additional losses and decreases fan performance. At an inlet length of $L_{Inlet}/D_{Fan} \approx 1.9$ the shock within the inlet as well as at the start of the ramp in the full-scale configuration significantly reduced and completely vanished at the second highest tested inlet length. As the initial shock at the inlet ramp and the intake shock afterwards couldn't be replicated in the model case with applied velocity ratio scaling, the larger deviation of the DC60 value between this configuration and the full-scale set-up can be explained. As the shock reduces/vanishes, it can be seen that the distortion factor between this model set-up and the full-scale configuration start to align better.

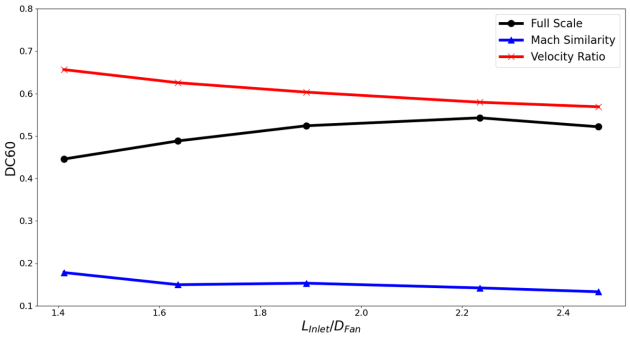

FIG 18. DC60 Values for different inlet lengths and model scaling

6. CONCLUSION

The study of the preliminary engine design identified a desirable selection of engine parameters for a UHBR engine with the objective of minimizing specific fuel consumption. In this approach of improving the design point thermodynamic cycle, the engine sizing was described for the conceptual analysis of the heavily-buried propulsor-airframe configuration.
The study pointed out the blockage effect associated with BLI and compensated that by increasing the inlet area. The different scaling approaches chosen for the engine conditions provided strongly different results. Applying Mach similarity to reach identical fan tip Mach numbers between the model and the full-scale configuration resulted in larger shock development compared to the full-scale case. Additionally, the overall flow field is altered significantly. The scaling done by velocity ratio captures this much better, despite the difference in Reynolds number, however it sacrifices the similarity in fan tip speed. Regardless of the scaling applied, the model configurations couldn't capture potential shocks further upstream due to the much lower freestream velocity of the wind tunnel. Specifically, shock occurrence at the start of the intake ramp proved to have significant impact on the flow field directly at the leading edge of the nacelle, promoting an additional inward lip shock at this location. Despite the change in the local flow field, additionally this can be seen in the inlet distortion coefficient, being lower with the existence of shock areas. Applying the velocity ratio scaling not only captures the overall flow field more accurately, but it also depicts the DC60 value better, but it significantly falls short when a shock forms at the inlet ramp, as it cannot replicate this phenomenon and fails to capture the secondary shock formation at the nacelle in those cases.
To properly design a wind tunnel model to capture the characteristics of BLI in a full-scale configuration, shock formations directly upstream of the intake have to be prevented, as they heavily impact the local flow field towards the propulsor and couldn't be captured by the chosen wind tunnel set-ups. The

scaling approaches chosen address different aspects to be investigated. Namely, similarity in fan behavior and similarity in the local flow field respectively. As it was not possible to satisfy both with the given set-up, further investigation is needed and consideration as to what extent important aspects of BLI are impacted with either of them, in order to settle for one approach. Additionally, an adjustment of the scaling to take the difference in Reynolds number into account will be investigated in the future. It has to be mentioned, that this paper only analysed the mid cruise condition. As the flow speed within the wind tunnel is limited to much lower Mach numbers, this complicates the problem at hand, clearly shown in the analyses done in this paper. Changing the operation point to take off or climb phases, allows for a closer match between the wind tunnel conditions and that of the full scale configuration. Hence, additional analyses are needed to understand the full problem, as well as design the wind tunnel experiment.
Moreover, the local loss generation mechanisms are a major open challenge that has yet to be addressed, as they remain poorly understood. Future work will involve detailed flow analyses in combination with newly developed, loss-specific post-processing will be carried out to address this knowledge gap.

7. ACKNOWLEDGEMENT

Funded by the Deutsche Forschungsgemeinschaft (DFG, German Research Foundation) - Project ID 498601949 - TRR 364

The authors gratefully acknowledge the computing time made available to them on the high-performance computer Lise at the NHR Center ZIB. This center is jointly supported by the Federal Ministry of Education and Research and the state govern- ments participating in the NHR (www.nhr-verein.de/unsere-partner)

Contact address:

manuel.zeitler@tu-braunschweig.de

References

[1] L. H. Smith. Wake ingestion propulsion benefit. *Journal of Propulsion and Power*, 9:74–82, 1993. ISSN: 07484658. DOI: 10.2514/3.11487.

[2] D. K. Hall, A. C. Huang, A. Uranga, E. M. Greitzer, M. Drela, and S. Sato. Boundary layer ingestion propulsion benefit for transport aircraft. *Journal of Propulsion and Power*, 33:1118–1129, 2017. ISSN: 15333876. DOI: 10.2514/1.B36321.

[3] S. A. Pandya, A.r Huang, A. Uranga, H. D.s Akaydin, and S. Moini-Yekta. The d8 aircraft: An aerodynamics study of boundary layer and wake ingestion benefit. 2015.

[4] AIRBUS. Airbus zeroe: Zeroe concept aircraft, Inspected 29.08.2024. https://www.airbus.com/en/innovation/energy-transition/hydrogen/zeroe.

[5] N. G.M. Moirou, D. S. Sanders, and P. Laskaridis. Advancements and prospects of boundary layer ingestion propulsion concepts, 4 2023. DOI: 10.1016/j.paerosci.2023.100897.

[6] A. Vinz and A. Raichle. Investigation of the effects of bli engine integration on aircraft thrust requirement. *CEAS Aeronautical Journal*, 15:1235–1250, 2024. DOI: 10.1007/s13272-024-00722-0.

[7] Institute of Aerodynamics and Flow Technology of the DLR. Unstructured computational fluid dynamics (cfd) solver for aerospace applications in research and industry in germany and europe, last checked December 2024. https://www.dlr.de/en/as/research-and-transfer/software-solutions/aerodynamics/software-tau.

[8] D. Giesecke, M. Lehmler, J. Friedrichs, J. Blinstrub, L. Bertsch, and W. Heinze. Evaluation of ultra-high bypass ratio engines for an over-wing aircraft configuration. *Journal of the Global Power and Propulsion Society*, 2:493–515, 2018. DOI: 10.22261/JGPPS.8SHP7K.

[9] J. Bijewitz, A. Seitz, and M. Hornung. Architectural comparison of advanced ultra-high bypass ratio turbofans for medium to long range application. *Deutscher Luft- und Raumfahrtkongress*, 2014. DocumentID: 340105.

[10] L. Benjamin, J. Friedrichs, P. Wegener, C. O. Marquez Gutierrez, and C. Heykena. Nacelle 3d aerodynamic design and airframe integration for an over wing configuration. *AIAA SCITECH 2023 Forum*, page 1651, 2023. 10.2514/6.2023-1651.

[11] D. L. Daggett, R. Kawai, and D. Friedman. Blended wing body systems studies: Boundary layer ingestion inlets with active flow control, 2003. http://www.sti.nasa.gov.

[12] T. Eggers. Zur 3d-schaufelgestaltung und zum abstroemverhalten des eintrittsleitrades einer modernen uhbr-fanstufe. Technical report, Technische Universitaet Braunschweig, Niedersaechsisches Forschungszentrum fuer Luftfahrt, 2023. ISBN 978-3-947623-64-8.

[13] J. Wild, M. Pott-Pollenske, and B. Nagel. An integrated design approach for low noise exposing high-lift devices. In *Collection of Technical Papers - 3rd AIAA Flow Control Conference*, volume 1, pages 17–32. American Institute of Aeronautics and Astronautics Inc., 2006. ISBN: 1563478137. DOI: 10.2514/6.2006-2843.

[14] D.L. Rodriguez. Multidisciplinary optimization method for designing boundary-layer- ingesting inlets. *Journal of Aircraft*, 46:883–894, 2009. ISSN: 15333868. DOI: 10.2514/1.38755.

[15] J. Pecinka, G. T. Bugajski, P. Kmoch, and A. Jilek. Jet engine inlet distortion screen and descriptor evaluation. *Acta Polytechnica*, 57:22–31, 2017. ISSN: 18052363. DOI: 10.14311/AP.2017.57.0022.